Shape and strain-induced magnetization reorientation and magnetic anisotropy in thin film Ti/CoCrPt/Ti lines and rings

D. Navas,[1,2] C. Nam,[1] D. Velazquez,[3] and C. A. Ross[1]
[1]*Materials Science and Engineering Department, MIT, Cambridge, Massachussets 02139, USA*
[2]*Departamento de Química-Física, Universidad del País Vasco, Leioa, 48940 Vizcaya, Spain*
[3]*Felguera-IHI SA, Las Rozas, 28232 Madrid, Spain*

(Received 28 January 2010; revised manuscript received 16 April 2010; published 30 June 2010)

The contributions to the magnetic anisotropy of thin-film rings and lines of width 50 nm and above made from Ti(5 nm)/$Co_{0.66}Cr_{0.22}Pt_{0.12}$ (10 and 20 nm)/Ti (3 nm) with a perpendicular magnetocrystalline anisotropy are investigated, using magnetic force microscopy to image the ac-demagnetized state. Four regimes of behavior were observed in both lines and rings. Samples with the largest widths (>500 nm) showed an out-of-plane maze domain structure typical of unpatterned films with domain widths of ~200 nm. As the linewidth decreased, a "bamboo" domain structure forms in which the domain walls lie approximately perpendicular to the linewidth. Further linewidth decreases result in a reorientation to a net in-plane anisotropy perpendicular to the linewidth, and for the narrowest lines, <200-nm wide, the anisotropy reorients in plane parallel to the line. The evolution of anisotropy is modeled in terms of contributions from magnetocrystalline, shape, and first- and second-order magnetoelastic terms, and good agreement with experiment is obtained, considering both bulk and surface anisotropy contributions.

DOI: 10.1103/PhysRevB.81.224439 PACS number(s): 75.30.Gw, 75.70.Kw, 68.37.Rt, 75.75.−c

I. INTRODUCTION

Ferromagnetic thin films with out-of-plane magnetic anisotropy have been widely studied for perpendicular magnetic recording media applications[1,2] as well as for patterned magnetic media.[3–6] More recently, magnetic films patterned into stripes have been proposed for data storage[7] and logic applications,[8] and films with perpendicular anisotropy may be advantageous in these applications due to a lower critical current for current-induced domain-wall motion.[9–15] Thin-film magnetic rings are also of considerable interest in nonvolatile multibit memory, biosensors, and logic devices based on giant magnetoresistence,[16–19] although rings with perpendicular anisotropy have not been explored.

In patterned magnetic films, net anisotropy is determined by the magnetocrystalline (MC) anisotropy, the shape (SH) anisotropy, and magnetoelastic (ME) effects due to the high strain commonly found in thin films grown on substrates.[20] Moreover, in addition to the bulk-anisotropy terms, surface (SU) terms must also be considered. The reduced symmetry of surface atoms as compared to bulk atoms gives rise to a uniaxial magnetic surface anisotropy known as a Néel-type anisotropy, different from the bulk value.[21–23] Surface or interface anisotropies are expected to be significant for thin films, multilayers, and patterned structures, affecting their reversal process and remanent states.[20,24] Therefore, understanding the various contributions to anisotropy as a function of the dimensions of the thin film when it is patterned is the key to obtaining the desired anisotropy, whether it be perpendicular or in plane, in order to use these materials in a range of magnetic devices.

Perpendicular anisotropy was observed in thin NiFe films on Cu(111) in 1968 (Ref. 25) and subsequently in a range of other systems such as epitaxial bcc Fe/Ag(001),[26–30] fcc Fe/Cu(001),[31–35] Co/Au(111) thin films and superlattices,[36,37] Ni/Cu(001),[38–40] and Cu/Ni/Cu(001) sandwiches.[41,42] The combination of shape anisotropy energy, bulk magnetoelastic anisotropy, and the surface magnetocrystalline and magnetoelastic anisotropy terms can lead to a net perpendicular anisotropy.[43–45] However, as the thickness of the magnetic layer is increased, the anisotropy reorients in plane as shape anisotropy dominates, so perpendicular magnetization is limited to a range of thickness, e.g., from 2 to 13 nm for the Ni layer in epitaxial Cu/Ni/Cu sandwiches.[41,42] Perpendicular anisotropy can be obtained for thicker films by using a multilayer system[46–48] or by relying on an out-of-plane magnetocrystalline anisotropy such as that of hcp Co (Refs. 49 and 50) or tetragonal $L1_0$ structured FePt (Ref. 51) and FePd.[52,53] In this work, we selected a cobalt-platinum alloy ($Co_{0.66}Cr_{0.22}Pt_{0.12}$) due to its strong uniaxial magnetocrystalline anisotropy and the ability to orient the crystalline *c* axis out of plane by epitaxial growth onto a Ti(0001) underlayer. This alloy has been extensively studied for hard-disk data-storage applications.[54,55] Pt substitutes for Co in the hcp structure, increasing both the lattice constant and the magnetocrystalline anisotropy.[56,57]

It is well known that patterning of a strained layer breaks the in-plane symmetry and produces an asymmetric strain relaxation, and changes the magnetoelastic anisotropy. There has been considerable work on patterned lines with perpendicular anisotropy,[10–15,58–60] but in most cases, the contributions of the magnetoelastic and surface anisotropy terms have not been considered. However, both terms have been shown to be important components of the net anisotropy, and in fact, they can dominate in certain cases such as patterned Cu/Ni/Cu stripes.[61–64] Domain size is also important, and both theoretical[60,65] and experimental[66] studies of nanolines with perpendicular anisotropy have shown that both the size and the orientation of the stripe domains depend on the lateral size of the wire.

In this paper, we analyze the magnetic-anisotropy contributions of patterned and unpatterned films of sputtered

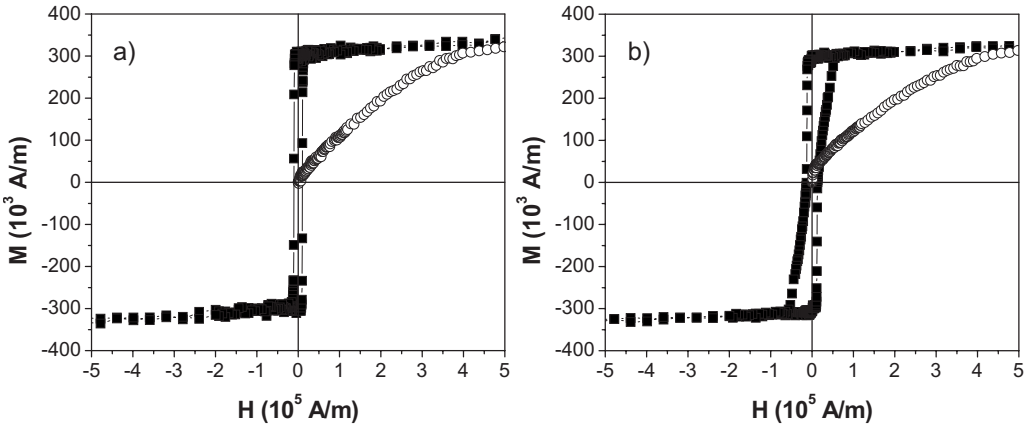

FIG. 1. Out-of-plane hysteresis loops (■) and in-plane virgin curves (○) of (a) 10-nm-thick and (b) 20-nm-thick $Co_{0.66}Cr_{0.22}Pt_{0.12}$ films.

$Ti/Co_{0.66}Cr_{0.22}Pt_{0.12}/Ti$ with perpendicular magnetocrystalline anisotropy. The net magnetic anisotropy energy of unpatterned films is treated as a combination of bulk and surface anisotropy terms. Changes in the anisotropy as a function of linewidth and thickness are analyzed, and a reorientation from perpendicular to in-plane transverse to the wires, and to in-plane parallel to the wires, is explained. In thin-film rings, this enables the magnetization to be oriented out of plane, in plane in the radial direction, or in plane around the ring circumference.

II. EXPERIMENTAL METHODS

A 5-nm Ti seed layer, a 10- or 20-nm-thick Co66 at. %/Cr22 at. %/Pt12 at. % (CoCrPt) film, then a 3-nm Ti capping layer were deposited sequentially on (100) Si wafers with native oxide by rf sputtering. Patterned line and ring structures were made by standard electron-beam lithography, sputter-deposition, and lift-off techniques. Electron-beam lithography was performed at 10 keV to define a pattern in 950 kg/mol polymethylmethacrylate resist, followed by developing the samples in a mixture 1:3 of methyl isobutyl ketone and isopropyl alcohol. The Ar (99.999% pure) sputtering gas pressure was 2 mTorr, the base pressure was below 2×10^{-8} Torr, and the rf power was 300 W for 5-cm-diameter targets.[67,68] The deposition rates were 1.9 Å/s for CoCrPt and 0.8 Å/s for Ti. The lift-off procedure was carried out by submerging the sample in N-methyl-2-pyrrolidone at 135 °C, followed by an ultrasonic bath. Line patterns had lengths of 10 μm and widths from 100 nm to 2 μm while circular rings had an outer diameter of 3 μm and a linewidth from 50 nm to 1.25 μm. 3-μm-diameter circular disks were also made for comparison.

Characterization was performed by high-resolution scanning electron microscopy (HRSEM) in a JEOL 6320FV, and atomic and magnetic force microscopy (AFM and MFM) in a Veeco/Digital Instruments Nanoscope IIIa using low-moment Veeco tips with a cobalt/chromium coating. The tip was magnetized along its axis using a permanent magnet and the images were obtained in the vibrating-lift mode. The tip was kept at a constant distance of 30 nm above the surface of the sample for MFM imaging. The samples were initially ac demagnetized, applying the external magnetic field perpendicular to the sample plane. First the sample was saturated with an out-of-plane field of +800 kA/m, then alternating positive and negative fields were applied. The field value of each step is 0.9 times that of the previous one. Magnetic hysteresis loops were measured using a vibrating sample magnetometer (ADE model 1660). Virgin curves were measured from the ac-demagnetized state. All studies were done at room temperature. The strain distributions of the patterned films were studied by three-dimensional (3D) finite element modeling (FEM) using the commercial ANSYS mechanical simulator.

III. RESULTS

A. Unpatterned films

Figure 1 shows out-of-plane hysteresis loops and in-plane virgin curves of 10- and 20-nm-thick CoCrPt films. Magnetic measurements and x-ray diffractometry of similar CoCrPt films[68–70] indicate that the crystallographic c axis and the easy magnetization axis are oriented out of plane. While the out-of-plane hysteresis loop is almost square for the 10-nm-thick film, the 20-nm-thick film shows a slow approach to saturation which is attributed to the existence of small bubble domains that are magnetostatically stabilized by the surrounding regions. Coercive fields are 10.1×10^3 and 13.3×10^3 A/m for 10-nm-thick and 20-nm-thick films, respectively. The effective magnetic anisotropy energy (K^{eff}) can be estimated from the area between the magnetization-field (M-H) curve and the M axis when the external magnetic field is applied along the hard (i.e., in-plane) direction.[71] The in-plane virgin curves give K^{eff} values of $(7.2\pm0.4)\times10^4$ and $(7.4\pm0.3)\times10^4$ J/m^3 for 10- and 20-nm-thin film thicknesses, respectively. The saturation magnetization was determined from the hysteresis loops to be $M_s\approx(325\pm1)\times10^3$ A/m, in agreement with previous data.[69]

The ferromagnetic domain structure of 20-nm-thick CoCrPt film imaged by MFM is shown in Figs. 2(a) and 2(b). (Results from the 10-nm-thick film are not shown because the MFM tip significantly modified the domain pat-

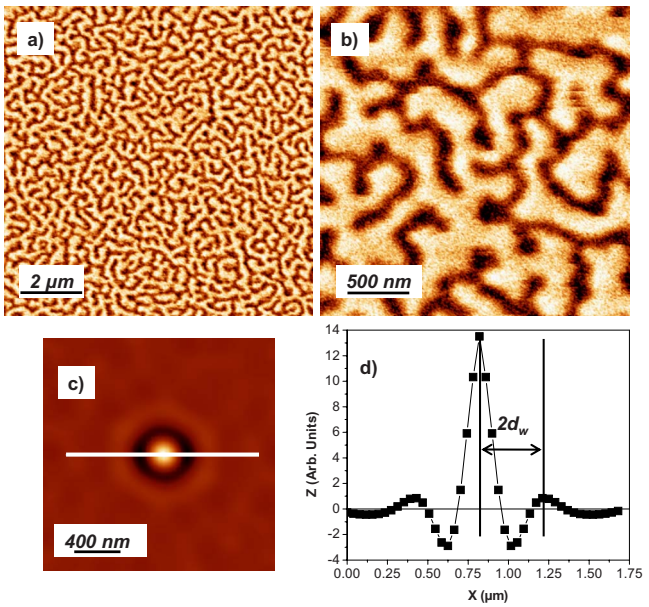

FIG. 2. (Color online) [(a) and (b)] MFM images of 20-nm-thick CoCrPt film on a smooth substrate after an ac-demagnetization process at different magnifications. (c) The autocorrelation map of image (a); and (d) a profile along the white line in (c). The distance between the main and the secondary maximums is the double of the average domain size ($2d_w = 180$ nm).

terns). Stripe domains are seen, typical of systems in which the magnetization is perpendicular to the plane of the substrate. An estimation of the period of the MFM images (i.e., twice the domain size) was obtained from the profile [Fig. 2(d)] of the self-correlation transform of the MFM images [Fig. 2(c)].[72] The maze domains have an average width (d_w) of 180 nm.

Kaplan and Gehring[73] predicted an evolution of the domain size with film thicknesses and Gehanno *et al.*[74] demonstrated that this prediction was valid when domain widths (d_w) are larger than film thickness (t). As our domain widths are nine times larger than the film thickness (t), the evolution of domain size is given by[75]

$$ln\left(\frac{d_w}{t}\right) = \frac{\pi D_0}{2t} + ln(\pi) - 1 + \mu\left[\frac{1}{2} - ln(2)\right] \qquad (1)$$

for $(d_w/t) > 1.5$, where

$$\mu = 1 + \frac{M_s^2}{2\mu_0 K_u} \qquad (2)$$

and $D_0 = \sigma_w/(2\pi M_S^2)$, σ_w, M_s, μ_0, and K_u represent the dipolar length,[73,74] the domain-wall energy per unit area, the saturation magnetization, the permeability of free space ($4\pi \times 10^{-7}$ N/A^2), and uniaxial anisotropy constant (given by K^{eff} above), respectively. Substituting for M_s, K_u, d_w, and t, we find $D_0 = 30 \pm 4$ nm for the 20-nm-thick CoCrPt film, and $d_w = 1.0 \pm 0.3$ μm is the expected domain width for the 10-nm-thick CoCrPt film. In comparison, measurements by Keitoku *et al.*[76] gave domain sizes of 90–95 nm for 15- and 30-nm-thick $Co_{0.61}Cr_{0.13}Pt_{0.26}$ films, but domains of ~250 nm for 10-nm-thick films, which were unaffected by the MFM tip due to the high coercivity (87.6 kA/m) of the alloy.

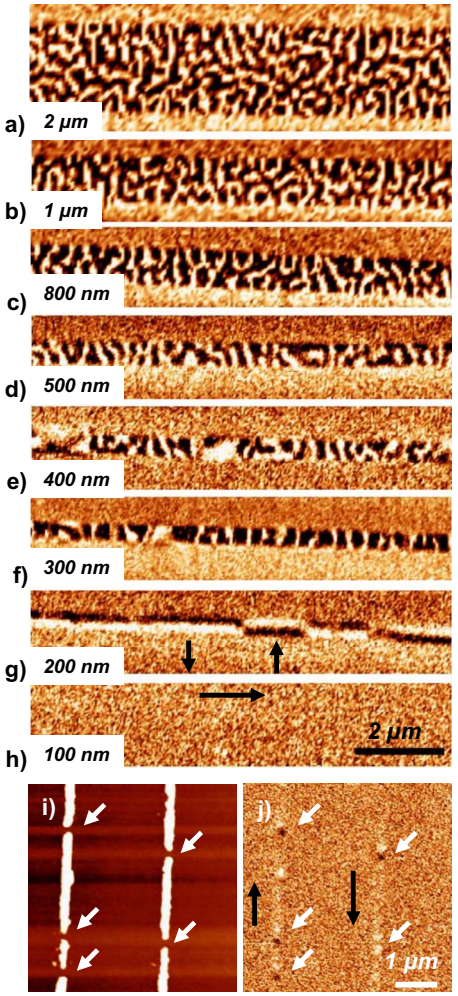

FIG. 3. (Color online) MFM images of 20-nm-thick CoCrPt lines with different widths: (a) 2 μm, (b) 1 μm, (c) 800 nm, (d) 500 nm, (e) 400 nm, (f) 300 nm, (g) 200 nm, and (h) 100 nm. (i) AFM and (j) MFM images of 20-nm-thick CoCrPt line arrays with 100 nm width, showing the effect of breaks in the lines. Black arrows indicate the in-plane magnetization directions in (f)–(h).

B. Patterned films: Lines and rings

Figure 3 shows MFM images of 20-nm-thick CoCrPt lines with different widths after ac demagnetization. The width varied from 2 μm [Fig. 3(a)] to 100 nm [Fig. 3(h)]. Stripe domains similar to the unpatterned film were observed for the wider lines [Figs. 3(a) and 3(b)]. However, the domain walls are aligned approximately perpendicular to the edges of the stripes, in agreement with a theoretical model which shows that the magnetic energy of the system is minimized when the domain walls are either transverse or parallel to the edge[77] so that domains with random orientations are likely to evolve toward a transverse configuration. Lee *et al.*[66] confirmed these predictions in evaporated Ni stripes with perpendicular anisotropy, where the domains oriented transverse to the stripe as stripe width decreased.

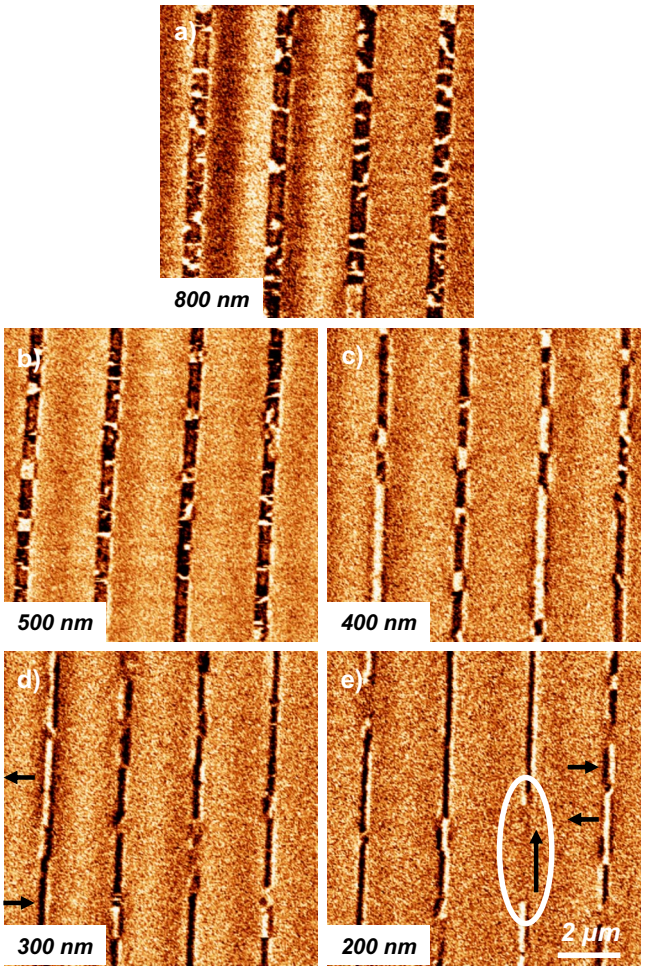

FIG. 4. (Color online) MFM images of 10-nm-thick CoCrPt line arrays with different widths: (a) 800 nm, (b) 500 nm, (c) 400 nm, (d) 300 nm, and (e) 200 nm. The white ellipse in (e) indicates a region of magnetization parallel to the line. Black arrows indicate the in-plane magnetization directions in (d) and (e).

Measurements of several wires of each width in the range of 400 nm–2 μm gave reproducible average domain sizes of ~180 nm, as seen in the unpatterned film. The transverse orientation of domain walls becomes clearer as the stripe width decreases, and for the 300-nm-wide stripe a "bamboo" structure is obtained [Fig. 3(f)] where the domains span the width of the stripe. However, below 300 nm linewidth, a transition from out-of-plane to in-plane magnetic domains lying perpendicular to the line axis was seen. The dark and light contrasts at the edges of the 200-nm-wide stripe [Fig. 3(g)] is consistent with transverse in-plane magnetization in which the domains are several micron long. Finally, lines with 100 nm width [Fig. 3(h)] showed no MFM contrast. This is attributed to a second reorientation leading to a magnetization parallel to the stripe. This is confirmed by imaging breaks in the wire [Figs. 3(i) and 3(j)] at which magnetic contrast is visible. For clarity, the in-plane magnetization directions (both transverse and parallel to the line axis) have been indicated by black arrows in Figs. 3 and 4.

Similar trends are found in the 10-nm-thick CoCrPt lines (Fig. 4). For the wider lines with perpendicular anisotropy,

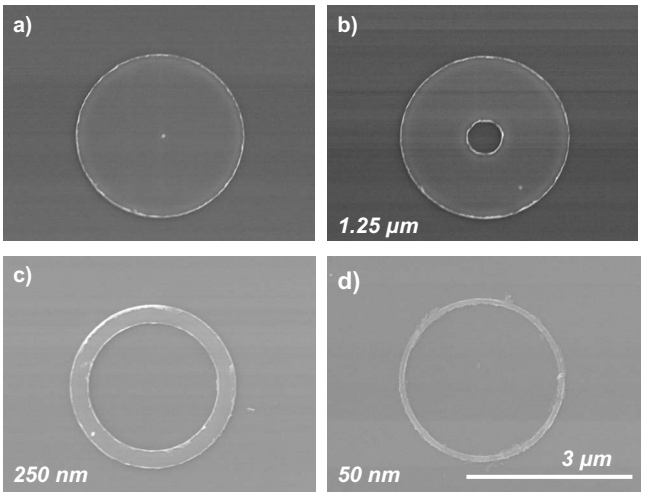

FIG. 5. HRSEM images of (a) CoCrPt disk and [(b)–(d)] rings with 3-μm external diameter. The line widths of the rings range from 1.25 μm to 50 nm. Examples with (b) 1.25-μm, (c) 250 nm, and (d) 50 nm widths are shown in this figure.

the MFM tip disturbs the domains, as is evident by the greater preponderance of dark (attractive) contrast in the MFM images. Despite this, it is clear that the 800- and 500-nm-wide structures have a net perpendicular anisotropy with a bamboo domain structure. This reorients to an in-plane transverse magnetization (seen for 400-, 300- and 200-nm-wide stripes). The transverse domains appear not to be disturbed by the tip. At 200 nm width, contrastless regions with an in-plane magnetization parallel to the line are present, as indicated by an ellipse in Fig. 4(e). These results show that for the 10-nm-thick CoCrPt, the anisotropy reorientations occur at wider linewidths than for the 20-nm-thick CoCrPt. Imaging different areas of the samples and several scans of the same area confirm that the domain configurations are not experimental artifacts.

We now describe the magnetic states of 10- and 20-nm-thick CoCrPt disk and rings after ac demagnetization. Examples of the rings are given in Fig. 5. Figures 6(a)–6(f) show MFM data from 20-nm-thick samples. Stripe domains are observed for disks [Fig. 6(a)] and wide rings [Fig. 6(b)] with the walls orienting perpendicular to the line edge as the linewidth decreases [Figs. 6(c) and 6(d)]. At 250 and 200 nm linewidths [Figs. 6(e) and 6(f)], coexisting perpendicular bamboo domains (dark arrow) and transverse or radial (white arrow) magnetized domains coexist, with transverse domains predominating as the linewidth decreases. Rings with linewidths of 50 and 100 nm showed no contrast, indicating a circumferential magnetization. These rings exhibit a "vortex" or flux-closed state without domain walls, as seen in rings made from in-plane magnetized thin films.[78]

Figures 6(g)–6(j) show corresponding data for 10-nm-thick films. A bamboo domain structure, with domain length on the order of 1 μm, exists in rings with 500 nm width [Fig. 6(g)], but the magnetization reorients to a transverse direction at 250 nm linewidth [Fig. 6(h)]. A combination of in-plane magnetic domains lying parallel [black arrows in Fig. 6(i)] and transverse to the ring edge is found in rings with 200 nm width. Finally, no contrast was measured for the

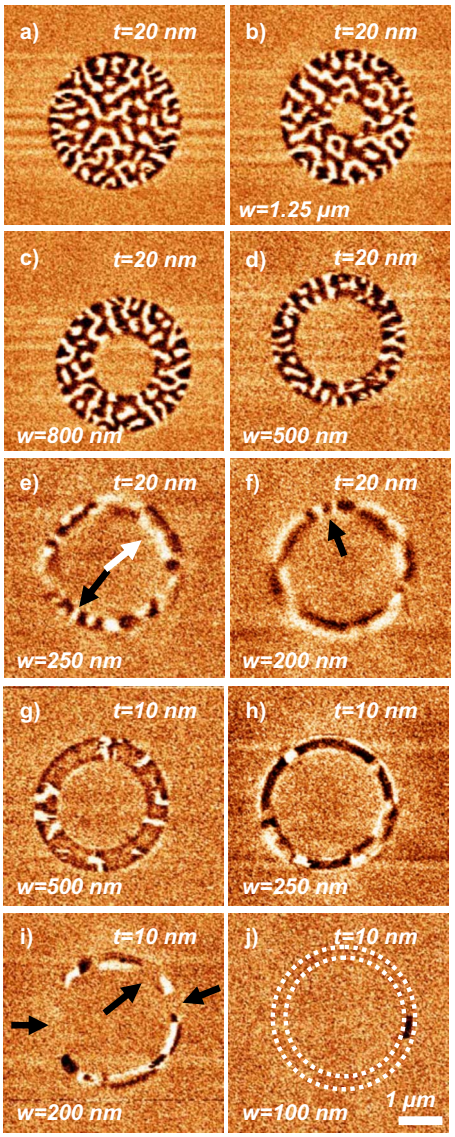

FIG. 6. (Color online) MFM images of (a) 20-nm-thick CoCrPt disk and [b)–(f)] rings with 3-μm external diameter. The line widths of the rings range from 1.25 μm to 200 nm. Examples with (b) 1.25-μm, (c) 800-nm, (d) 500-nm, (e) 250-nm, and (f) 200 nm widths are shown. Thickness t and width w are indicated on each image. MFM images of 10-nm-thick CoCrPt rings with 3-μm external diameter and the line widths of the rings are: (g) 500 nm, (h) 250 nm, and (i) 200 nm. (j) MFM image of 10-nm-thick CoCrPt ring with 3-μm external diameter and 100 nm wall width after in-plane saturation.

rings with 100 and 50 nm widths, again indicating a vortex state.

The observations for rings are consistent with those made on straight stripes. However, for the narrowest stripes with circumferential magnetization, the ring geometry provides for two possible magnetization states, the vortex state, where the magnetization runs circumferentially clockwise or counterclockwise without domain walls, and the onion state, where two 180° domain walls are present.[78–85] For rings with in-plane anisotropy, an onion state is typically formed at remanence after saturation in an in-plane field and the locations of the domain walls are determined by the magnetic field direction. A vortex state is then formed by applying a reverse field, causing the movement of one domain wall around the ring until it annihilates the other domain wall. To demonstrate the existence of onion states, rings of 100 nm width, and thickness 10 and 20 nm were magnetized in an in-plane field of 800 kA/m then imaged at remanence [Fig. 6(j)]. These images show contrast characteristic of an onion state. The 180° walls, which show as dark or light contrast, are disturbed by the tip and show as arcs extending part way around the ring.

IV. DISCUSSION

A. Anisotropy terms for unpatterned films of Ti/CoCrPt/Ti

The magnetic anisotropy energy for a thin film can be written as a sum of the MC, magnetostatic or SH, ME and SU anisotropy energies, i.e.,[20]

$$K^{eff} = K^{\mathrm{MC}} + K^{\mathrm{SH}} + K^{\mathrm{ME}} + K^{\mathrm{SU}} \tag{3}$$

in which positive values favor perpendicular magnetization and negative values favor in-plane magnetization.

Prior work gives K^{MC} of $\approx 37\times 10^4$ J/m^3 for a $Co_{73}Cr_{15}Pt_{12}$ single crystal and $\approx 24\times 10^4$ J/m^3 for $Co_{69}Cr_{19}Pt_{12}$ at room temperature.[69] By a linear extrapolation, we obtain a value for the alloy used here of $K^{\mathrm{MC}} = 17.5\times 10^4$ J/m^3, which is assumed independent of film thickness. The shape anisotropy energy of a thin film is negative and has magnitude

$$K^{\mathrm{SH}} = \frac{\mu_0 M_S^2}{2} = (6.6 \pm 0.3) \times 10^4 \ \mathrm{J/m^3}. \tag{4}$$

The bulk first-order magnetoelastic-anisotropy term may be written by[71]

$$K^{\mathrm{ME}} = K_1^{\mathrm{ME}} = \frac{3}{2}\lambda_S \Delta\sigma, \tag{5}$$

where λ_S is the saturation magnetostriction constant and $\Delta\sigma$ is the difference in stress measured along two orthogonal directions, σ^{in_plane} and σ^{axial}. If we assume that $\sigma^{axial}=0$ due to relaxation at the free surface, then K^{ME} is proportional to σ^{in_plane}. The stress arises from the misfit between the lattice parameters of thin film and the Ti underlayer. The lattice mismatch strain between an epitaxial film and an underlying substrate (here Ti) is determined by $\eta=(a_S-a_F)/a_S$, where a_S and a_F are the substrate and film in-plane lattice constants, respectively. The lattice parameters of $Co_{0.71}Cr_{0.19}Pt_{0.10}$ and Ti are 2.57 Å (Ref. 86) and 2.95 Å, respectively. This gives a lattice mismatch of 0.1288 (12.9%), if we assume that the Ti is unstrained. However, in the present case, where Ti and CoCrPt films have similar thicknesses, strain will be present in both layers. We approximate the situation to that of a general multilayer A/B, in which both layers adopt the same in-plane lattice parameter. The strain is described by[43]

$$\varepsilon_x = \varepsilon_y = \varepsilon = \eta/(1 + t_{\mathrm{CoCrPt}}E_{\mathrm{CoCrPt}}/t_{\mathrm{Ti}}E_{\mathrm{Ti}}), \tag{6}$$

where E and t are the Young's modulus and thickness of CoCrPt and Ti films, respectively. The Young's moduli are

about 200 GPa (Ref. 87) and 116 GPa for CoCrPt and Ti, respectively. The film thicknesses are 5 nm for Ti films and 10 and 20 nm for CoCrPt layers. Substituting these values in Eq. (6), the predicted in-plane strains are 0.02895 (2.9%) and 0.01631 (1.6%) for 10- and 20-nm-thick CoCrPt films. This result for the magnitude of the strain assumes that there is no strain relief by the formation of misfit dislocations in the film. For films above a critical thickness t_c, the film strain relaxes toward zero with increasing thickness.[45,88] Measurements of t_c in other systems give $t_c=2$ nm for Co(0001) on W(110) with misfit strain 3%,[89] t_c at least 10 nm for Co(0001) on Mo(110) with misfit 2.4% (Ref. 50) and t_c of order 30 nm for CoCrPt on Ti/CoZr.[90] In the following calculations, strain relief has been neglected, and the magnetoelastic contributions therefore represent an upper bound.

From the in-plane strain, biaxial stress is given by[91,92]

$$\sigma^{in\_plane} = [E_{\mathrm{CoCrPt}}/(1-\nu_{\mathrm{CoCrPt}})]\varepsilon^{in\_plane}_{\mathrm{CoCrPt}}, \tag{7}$$

where ν_{CoCrPt} is the Poisson ratio, 0.32 for Co. Under these assumptions, the in-plane stresses are therefore 8.5 GPa and 4.8 GPa for 10-nm-thick and 20-nm-thick CoCrPt films, respectively.

A value for $\lambda_S \approx -5\times10^{-6}$ is assumed, although this can vary with film thickness and Pt content.[93] The negative λ_S and tensile (positive) stresses give a negative $\lambda_S\Delta\sigma$ and an out-of-plane easy axis of magnetization. Therefore, the bulk first-order magnetoelastic-anisotropy term [Eq. (5)] favors a perpendicular anisotropy with magnitude K_1^{ME} of 6.4×10^4 and 3.6×10^4 J/m^3 for 10-nm and 20-nm film thicknesses, respectively.

A surface anisotropy term may arise from Néel spin-orbit contributions or from strains that are localized at the surface.[20,21,94] In our case, surface-energy terms for a continuous thin film model arise from two surfaces, the Ti-CoCrPt interfaces on top and below the CoCrPt thin film, separated by a distance t, the CoCrPt film thickness. The surface contributions to magnetocrystalline and magnetoelastic energies are[20]

$$K^{\mathrm{SU}} = 2\left[\frac{K^{\mathrm{SU}}_{\mathrm{Ti\text{-}CoCrPt}}}{t} + \frac{B^{\mathrm{SU}}_{\mathrm{Ti\text{-}CoCrPt}}}{t}\varepsilon\right], \tag{8}$$

where $K^{\mathrm{SU}}_{\mathrm{Ti\text{-}CoCrPt}}$ and $B^{\mathrm{SU}}_{\mathrm{Ti\text{-}CoCrPt}}$ are the surface magnetocrystalline and magnetoelastic terms, respectively, t is the CoCrPt film thickness, and ε is the biaxial in-plane strain. Values of these parameters are not available for CoCrPt so we use the surface magnetocrystalline term of a Co thin film sandwiched between two Ti layers, 0.7 mJ/m^2.[95] The surface magnetocrystalline anisotropy energies are then $(14.0\pm0.7)\times10^4$ and $(7.0\pm0.2)\times10^4$ J/m^3 for 10- and 20-nm CoCrPt thin-film thicknesses. Surface magnetocrystalline anisotropy terms favor an out-of-plane magnetization direction. The value of the surface magnetoelastic term will be addressed below.

Finally, an additional higher-order magnetoelastic anisotropy term must be included when the misfit-induced strain is high [$\varepsilon(t)\geq1\%$], to account for nonlinear effects in addition to classical elasticity theory.[96] The nonlinear magnetoelastic anisotropy term is proportional to the second power of strain:

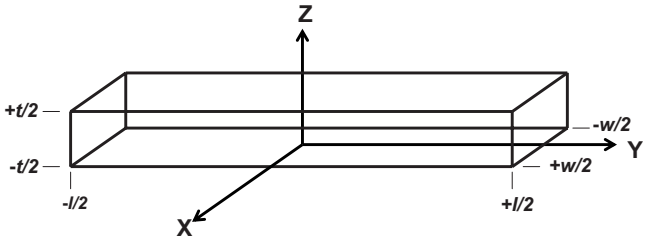

FIG. 7. Diagram of a nanoline with length l, width w, and thickness t.

$K_2^{\mathrm{ME}}=\varepsilon(t)^2h_2^{\mathrm{ME}}$. The physical origin for this second-order term (h_2^{ME}) lies in the strong tetragonal distortion (changes in the ratio c/a) of the hcp lattice due to the in-plane strain as the CoCrPt thickness decreases.[96] This term is not well understood but nonlinear effects have been included in the analysis of a range of systems that include ferromagnetic transition metals (Co and Ni) and rare earths.[44,50,89,94,96–99] Both surface and second-order parameters have been shown to be crucial in previous calculations such as for the Cu/Ni/Cu multilayer system.[94]

To obtain values for $B^{\mathrm{SU}}_{\mathrm{Ti\text{-}CoCrPt}}$ *and* h_2^{ME} we use the following expression, into which values are substituted for the 10-nm and 20-nm films:

$$K^{eff} = K^{\mathrm{MC}} + K^{\mathrm{SH}} + K_1^{\mathrm{ME}} + K_2^{\mathrm{ME}} + 2\left[\frac{K^{\mathrm{SU}}_{\mathrm{Ti\text{-}CoCrPt}}}{t} + \frac{B^{\mathrm{SU}}_{\mathrm{Ti\text{-}CoCrPt}}}{t}\varepsilon\right]. \tag{9}$$

Solving the two equations simultaneously yields (0.3 ± 0.1) J/m^2 for the surface magnetoelastic term $B^{\mathrm{SU}}_{\mathrm{Ti\text{-}CoCrPt}}$ and $(-2.4\pm0.4)\times10^9$ J/m^3 for the bulk second-order magnetoelastic anisotropy coefficient h_2^{ME}. It is important to note that our model omits terms of minor magnitude such as second- and higher-order magnetoelastic surface, and bulk magnetocrystalline anisotropy terms. Despite this, our fitted values are in the range of those values previously obtained for Co films.[50,89,99]

B. Anisotropy of Ti/CoCrPt/Ti lines and rings

A uniaxial model is inadequate to describe the lower symmetry of the patterned Ti/CoCrPt/Ti system. An anisotropy model for the patterned system needs to account for the nonequivalence of the in-plane directions, which affects both the magnetostatic and the magnetoelastic energies, giving three distinct anisotropy terms instead of the two for the thin-film system.[61,64] We use a Cartesian system with the x axis in plane but perpendicular to the long axis of the lines, the y-axis in-plane along the long axis and the z axis along the film normal (Fig. 7). The lines have length l, width w, and thickness t. For an infinite line length, longitudinal surface terms are negligible because $l\gg w$. Effective anisotropy terms are simply given by taking the difference between the energy terms, e.g., the XY anisotropy$=E_x-E_y$.

First, the shape anisotropy term is considered. Demagnetization factors have been estimated for prisms using the approximations reported by Aharoni.[100] Considering an isolated

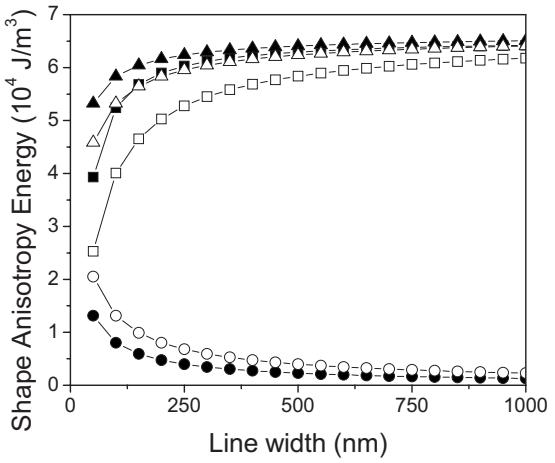

FIG. 8. Shape-anisotropy energy between two orthogonal directions (■ *ZX*, ▲ *ZY*, and ● *XY*) of an infinite CoCrPt line as a function of the width for 10-nm (solid symbols) and 20-nm (open symbols) film thicknesses.

line with infinite length ($l \rightarrow \infty$), the demagnetization factors are given by

$$N_x \approx 1 - N_z,$$

$$N_y = 0,$$

$$N_z = \frac{1}{\pi}\left[\frac{1-p^2}{2p}\ln(1+p^2) + p\,\ln(p) + 2\,\arctan\left(\frac{1}{p}\right)\right], \tag{10}$$

where $p=t/w$. The shape-anisotropy term is given by

$$K_{AB}^{\mathrm{SH}} = \frac{\mu_0(N_A - N_B)M_S^2}{2}, \tag{11}$$

where N_A and N_B are the demagnetizing factors in two orthogonal directions. Figure 8 shows the calculated shape anisotropy of CoCrPt lines with infinite length as a function of linewidth for 10 and 20 nm thicknesses.

The biaxial stress present in continuous Ti/CoCrPt/Ti thin films relaxes as the film is patterned due to transverse strain relaxation at the line edges. For a long line, the longitudinal strain is largely unchanged.[64,101] For example, 30-nm-thick Si films patterned into 90-nm-wide, millimeter-long lines are under approximately uniaxial strain with ~80% transverse strain relaxation and ~5% longitudinal strain relaxation,[101] while 10-nm-thick long Ni lines with 200-nm linewidth showed ~50% transverse strain relaxation and no longitudinal strain relaxation.[64] In the limiting case of long narrow lines, we assume that the strain in the *y* direction (parallel to the lines) is unchanged but that there is transverse strain relief in the *x* direction (in-plane perpendicular to the lines). Considering that the magnetostriction constant (λ_S) for CoCrPt is negative and stress is tensile (+) along the *y* direction, the *y* axis becomes a hard axis and the *XZ* plane, normal to the stress axis, an easy plane of magnetization. This resembles the effects of the relaxation of tensile strain in epitaxial Cu/Ni (10–15 nm)/Cu lines, which produced an easy axis in plane perpendicular to the lines.[64]

A FEM was used to calculate strain relaxation in CoCrPt films as a function of linewidth, based on an initial equibiaxial stress state of 4.8 GPa for unpatterned films with 20-nm thickness. The effect of the Ti capping layer was neglected and boundary conditions prescribe zero displacement at the lower surface of the CoCrPt in contact with the Ti underlayer. The system was equilibrated at a temperature at which the resulting thermal-expansion strain was equivalent to the CoCrPt/Ti misfit strain. Figures 9(a)–9(c) shows examples of the stress distribution in 20-nm-thick CoCrPt lines of different widths, indicating relaxation at the edges of wider lines and over much of the volume of narrower lines. The small regions with negative stress indicate compression. An estimation of the average strains along the *x* component $[\varepsilon^x(w)]$ as a function of the linewidths (w) has been summarized in Fig. 9(d). On the vertical axis, 100% represents the biaxial strain of an unpatterned film (ε^{in_plane}), and 0% indicates complete strain relaxation. The strain along the line axis (ε^y) is unchanged and equivalent to the biaxial strain ($\varepsilon^{in\_plane} = \varepsilon^y$). Substituting $\varepsilon^x(w)$ and ε^y in Eq. (7), stresses can be obtained as a function of the linewidths. The magnetoelastic anisotropy along the major axes can be calculated from the difference between the stress components. As a first approximation, similar strain relaxations along the *x* direction, obtained from the FEM for the 20-nm-thick films, were assumed for the 10-nm-thick samples.

The vertical sides of the patterned stripes also contribute to the surface-energy term. Both sides are assumed to be oxidized and the anisotropy-energy term is

$$K_Y^{\mathrm{SU}} = 2\left[\frac{K_{\mathrm{CoCrPt\text{-}O}}^{\mathrm{SU}}}{w}\right], \tag{12}$$

where $K_{\mathrm{CoCrPt\text{-}O}}^{\mathrm{SU}}$ is the surface magnetocrystalline energy corresponding to the CoCrPt-oxide interface, w is the linewidth, and the factor 2 originates from the two sides of the stripe. A value of $K_{\mathrm{CoCrPt\text{-}O}}^{\mathrm{SU}} = 3$ mJ/m^2 is taken based on measurements on the Co/CoO interface.[102,103]

In summary, the effective anisotropy energy of an infinite CoCrPt line in a plane defined by two orthogonal directions *A* and *B* as a function of the linewidth w and thickness t, is given by

$$K_{AB}^{eff} = K_{AB}^{\mathrm{MC}} + K_{AB}^{\mathrm{SH}} + K_{AB}^{\mathrm{ME}} + K_{AB}^{\mathrm{SU}} = K_{AB}^{\mathrm{MC}} + K_{AB}^{\mathrm{SH}} + K_{1AB}^{\mathrm{ME}}(w) + K_{2AB}^{\mathrm{ME}} + 2\left[\frac{K_{\mathrm{Ti\text{-}CoCrPt}}^{\mathrm{SU}}}{t} + \frac{B_{\mathrm{Ti\text{-}CoCrPt}}^{\mathrm{SU}}}{t}\varepsilon\right] + 2\left[\frac{K_{\mathrm{CoCrPt\text{-}O}}^{\mathrm{SU}}}{w}\right], \tag{13}$$

where ε is the biaxial strain prior to relaxation. The strain relief is introduced in Eq. (13) by the dependence of the magnetoelastic anisotropy term on the linewidth $[K_{1AB}^{\mathrm{ME}}(w)]$. A positive (negative) value indicates that the easy magnetization axis is parallel to the direction *A* (*B*). Effective anisotropy energies are shown in Fig. 10 for patterned thin films in different directions as a function of the linewidth and the continuous film as a reference.

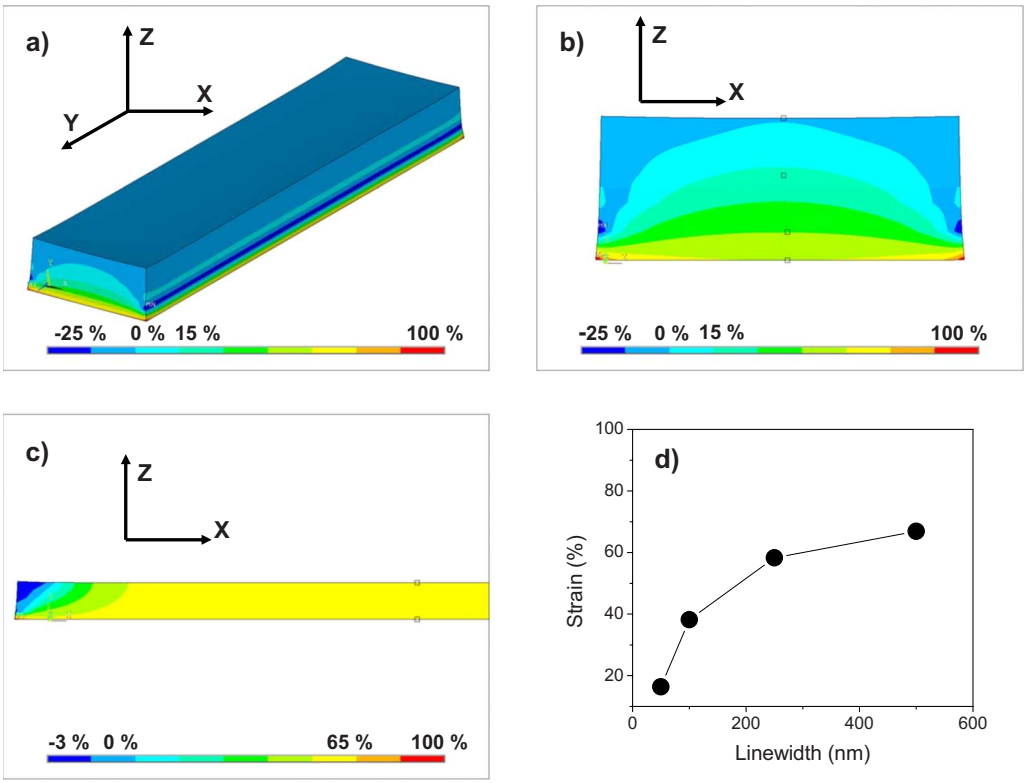

FIG. 9. (Color online) (a) 3D ANSYS simulated stress plots of 20-nm-thick lines with 50 nm width. The component parallel to the x axis is shown. [(b) and (c)] two-dimensional cross-section plots of the stress distribution in 20-nm-thick lines with (b) 50 nm and (c) 500 nm widths. (d) Strain along x as a function of the linewidth for 20-nm-thick films.

Considering the ZX anisotropy, the magnetocrystalline energy (K_{ZX}^{MC}) is positive but the shape anisotropy (K_{ZX}^{MC}) is negative. Surface magnetocrystalline ($K_{\mathrm{Ti\text{-}CoCrPt}}^{\mathrm{SU}}$) and magnetoelastic ($B_{\mathrm{Ti\text{-}CoCrPt}}^{\mathrm{SU}}$) terms also favor magnetization along the z direction but the second-order magnetoelastic (K_{2ZX}^{ME}) and surface magnetocrystalline ($K_{\mathrm{CoCrPt\text{-}O}}^{\mathrm{SU}}$) terms favor in-plane magnetization perpendicular to the line axis. For the narrowest lines, σ^X tends to 0, and since $\sigma^Z=0$, the contribution of the first-order magnetoelastic (K_{1ZX}^{ME}) term would be small.

For the XY anistropy, while the first-order magnetoelastic (K_{1XY}^{ME}), surface magnetoelastic ($B_{\mathrm{Ti\text{-}CoCrPt}}^{\mathrm{SU}}$) and magnetocrystalline ($K_{\mathrm{CoCrPt\text{-}O}}^{\mathrm{SU}}$) terms are positive, shape anisotropy (K_{XY}^{SH}) and second-order magnetoelastic (K_{2XY}^{ME}) terms are negative. As the "XY" plane is a hard magnetization plane for magnetocrystalline energy (K_{XY}^{MC}) and surface magnetocrystalline ($K_{\mathrm{Ti\text{-}CoCrPt}}^{\mathrm{SU}}$) terms, both contributions to K_{XY}^{eff} are zero.

The model (Fig. 10) therefore predicts a transition in the easy magnetization axis from along the z direction (out of plane) for the widest lines to the x direction (in plane perpendicular to the line axis) for intermediate linewidth. Finally, the magnetization reorients into the y direction (along the line axis) for the narrowest lines. The first reorientation from the z to the x direction is predicted to occur around 130 nm and 85 nm for 10-nm-thick and 20-nm-thick CoCrPt lines, respectively. The second reorientation into the y direction occurs at 50 nm and 60 nm, respectively.

We note that this model can also be applied to rings in which the linewidth is narrow compared to the diameter. Our phenomenological model (Fig. 10) was determined for lines with widths from 50 to 800 nm. As the external diameter of the rings is large (3 μm) and the strain relaxation depends only on the linewidth, we assume that the magnetic anisotropy energy of a ring can be treated in the same way as that of a line, provided the linewidth is much smaller than the ring diameter so that curvature of the ring is not significant. The same contributions to the anisotropy energy are relevant in rings but for a ring the in-plane preferred magnetization can lead to both the vortex and onion magnetic configurations which do not occur in a straight stripe.

C. Comparison with experiment

We saw earlier that for the 10-nm-thick CoCrPt films, the domain images imply an out-of-plane easy magnetization axis for linewidths larger than ≈300 nm. Between ≈300- and ≈200 nm width, the magnetization direction lies in plane, perpendicular to the line axis, and parallel to the line axis for widths below ≈200 nm. For the 20-nm-thick films, similar behavior is observed but the transitions occur at widths of ≈250 nm and ≈100 nm, respectively.

The model therefore explains qualitatively the changes in the easy-axis direction. However, in the model the transitions occur at lower values of linewidth, which means that the model predicts weaker in-plane anisotropy contributions than the experiment suggests. Discrepancies between the experimental data and modeling may be associated with both experimental and modeling limitations. The experiment does not give values of anisotropy directly, but instead measures

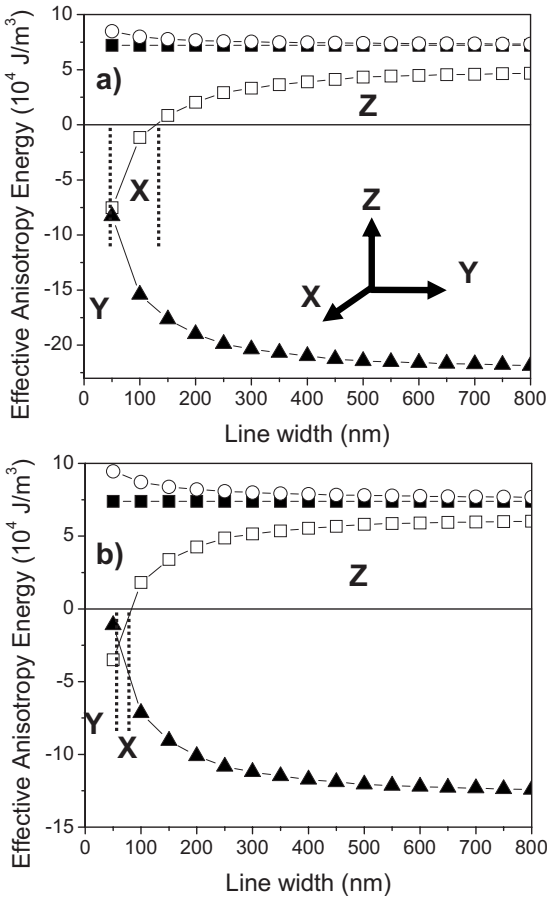

FIG. 10. Calculated effective anisotropy energy of continuous (■) and patterned thin films in different directions (□ for *ZX*, ○ for *ZY*, and ▲ for *XY*) as a function of the linewidth for (a) 10-nm and (b) 20-nm film thicknesses. *X*, *Y*, and *Z* indicate the linewidth regimes where the net anisotropy is transverse to the line in plane, along the line, and perpendicular to the line out of plane, respectively.

the remanent magnetization direction, as deduced from the stray-field distribution. The magnetization of the tip influences the magnetic state[104] and may enhance the apparent out-of-plane magnetization component. The model is itself limited by the neglect of the surface magnetoelastic anisotropy term ($B^{SU}_{CoCrPt\text{-}O}$), which would favor magnetization along the line length, and by neglect of terms of minor magnitude such as the second-order magnetoelastic surface and bulk magnetocrystalline anisotropy terms. It also neglects relaxation of misfit strain and therefore overestimates the magnetoelastic contributions. This would have the effect of lowering the predicted linewidth for the reorientation. In addition, the model uses parameters for Co, such as surface magnetocrystalline-anisotropy terms for Co/Ti and Co/CoO interfaces, instead of for CoCrPt/Ti and CoCrPt/CoCrPtO. However, in spite of these approximations, the model gives a good agreement with the experimental data and shows that a model including shape, magnetoelastic, magnetocrystalline, and surface-energy terms can predict the behavior of patterned magnetic films and allow the various anisotropy terms to be quantified.

V. SUMMARY

Two transitions of the easy magnetization axis (from out-of-plane to in-plane transverse to the line edge and then to in-plane along the line axis) have been experimentally observed in lines and rings made from a thin film with strong uniaxial magnetocrystalline anisotropy pointing perpendicular to the film plane, as the linewidth is decreased. The evolution of the anisotropy has been modeled in terms of contributions from bulk and surface terms. The model gives a good agreement with the experimental data. Our results suggest that the anisotropy transitions are mainly controlled by net changes in both shape and first-order magnetoelastic anisotropy energies occurring when the thin films were patterned. These results are relevant to a range of devices based on patterned magnetic films, where the net anisotropy is of key importance. For example, nanopatterned structures with perpendicular anisotropy, such as perpendicular spin valves, are important in magnetic memory or logic devices due to their high thermal stability and narrow domain-wall width, which enhances spin-torque efficiency. The model described here can be helpful in predicting the magnetic properties of patterned structures and contributing to the design and scaling of magnetic and magnetoelectronic devices.

ACKNOWLEDGMENTS

D.N. acknowledges support by the Spanish Ministry of Education and Culture and the Fulbright Commission. The authors acknowledge support by the MIT-Spain/La Cambra de Barcelona Seed Fund, the National Science Foundation and the INDEX program of the Nanoelectronics Research Initiative. The ANSYS simulator was courtesy of Felguera-IHI S.A.

[1] H. J. Richter, J. Phys. D **40**, R149 (2007).
[2] J. H. Judy, J. Magn. Magn. Mater. **287**, 16 (2005).
[3] B. D. Terris and T. Thomson, J. Phys. D **38**, R199 (2005).
[4] M. Albrecht, A. Moser, C. T. Rettner, S. Anders, T. Thomson, and B. D. Terris, Appl. Phys. Lett. **80**, 3409 (2002).
[5] K. Naito, Chaos **15**, 047507 (2005).
[6] C. A. Ross, Annu. Rev. Mater. Res. **31**, 203 (2001).
[7] S. S. P. Parkin, M. Hayashi, and L. Thomas, Science **320**, 190 (2008).
[8] D. A. Allwood, G. Xiong, C. C. Faulkner, D. Atkinson, D. Petit, and R. P. Cowburn, Science **309**, 1688 (2005).
[9] M. Yamanouchi, D. Chiba, F. Matsukura, and H. Ohno, Nature (London) **428**, 539 (2004).
[10] D. Ravelosona, D. Lacour, J. A. Katine, B. D. Terris, and C. Chappert, Phys. Rev. Lett. **95**, 117203 (2005).
[11] S. W. Jung, W. Kim, T. D. Lee, K. J. Lee, and H. W. Lee, Appl.

Phys. Lett. **92**, 202508 (2008).
[12] H. Tanigawa, T. Koyama, G. Yamada, D. Chiba, S. Kasai, S. Fukami, T. Suzuki, N. Ohshima, N. Ishiwata, Y. Nakatani, and T. Ono, Appl. Phys. Express **2**, 053002 (2009).
[13] E. Martinez, L. Lopez-Diaz, O. Alejos, and L. Torres, J. Appl. Phys. **106**, 043914 (2009).
[14] K. J. Kim, J. C. Lee, Y. J. Cho, C. W. Lee, K. H. Shin, S. Seo, K. J. Lee, H. W. Lee, and S. B. Choe, IEEE Trans. Magn. **45**, 3773 (2009).
[15] H. Szambolics, J. C. Toussaint, A. Marty, I. M. Miron, and L. D. Buda-Prejbeanu, J. Magn. Magn. Mater. **321**, 1912 (2009).
[16] R. Nakatani, T. Yoshida, Y. Endo, Y. Kawamura, M. Yamamoto, T. Takenaga, S. Aya, T. Kuroiwa, S. Beysen, and H. Kobayashi, J. Appl. Phys. **95**, 6714 (2004).
[17] J. Llandro, T. J. Hayward, D. Morecroft, J. A. C. Bland, F. J. Castano, I. A. Colin, and C. A. Ross, Appl. Phys. Lett. **91**, 203904 (2007).
[18] M. M. Miller, G. A. Prinz, S. F. Cheng, and S. Bounnak, Appl. Phys. Lett. **81**, 2211 (2002).
[19] F. J. Castaño, B. G. Ng, I. A. Colin, D. Morecroft, W. Jung, and C. A. Ross, J. Phys. D **41**, 132005 (2008).
[20] R. C. O'Handley, *Modern Magnetic Materials: Principles and Applications* (Wiley, New York, 2000).
[21] L. Néel, Acad. Sci., Paris, C. R. **237**, 1468 (1953); J. Phys. Radium **15**, 225 (1954).
[22] R. H. Victora and J. M. MacLaren, Phys. Rev. B **47**, 11583 (1993).
[23] U. Gradmann, J. Magn. Magn. Mater. **54-57**, 733 (1986).
[24] A. A. Leonov, U. K. Roßler, and A. N. Bogdanov, J. Appl. Phys. **104**, 084304 (2008).
[25] U. Gradmann and J. Muller, Phys. Status Solidi **27**, 313 (1968).
[26] N. C. Koon, B. T. Jonker, F. A. Volkening, J. J. Krebs, and G. A. Prinz, Phys. Rev. Lett. **59**, 2463 (1987).
[27] B. Heinrich, K. B. Urquhart, A. S. Arrott, J. F. Cochran, K. Myrtle, and S. T. Purcell, Phys. Rev. Lett. **59**, 1756 (1987).
[28] M. Stampanoni, A. Vaterlaus, M. Aeschlimann, and F. Meier, Phys. Rev. Lett. **59**, 2483 (1987).
[29] C. A. Ballentine, R. L. Fink, J. Araya-Poyet, and J. L. Erskine, Appl. Phys. A: Mater. Sci. Process. **49**, 459 (1989).
[30] Z. Q. Qiu, J. Pearson, and S. D. Bader, Phys. Rev. Lett. **70**, 1006 (1993).
[31] D. Pescia, M. Stampanoni, G. L. Bona, A. Vaterlaus, R. F. Willis, and F. Meier, Phys. Rev. Lett. **58**, 2126 (1987).
[32] C. Liu, E. R. Moog, and S. D. Bader, Phys. Rev. Lett. **60**, 2422 (1988).
[33] D. P. Pappas, K. P. Kamper, and H. Hopster, Phys. Rev. Lett. **64**, 3179 (1990).
[34] R. Allenspach and A. Bischof, Phys. Rev. Lett. **69**, 3385 (1992).
[35] J. Thomassen, F. May, B. Feldmann, M. Wuttig, and H. Ibach, Phys. Rev. Lett. **69**, 3831 (1992).
[36] C. H. Lee, H. He, F. J. Lamelas, W. Vavra, C. Uher, and R. Clarke, Phys. Rev. B **42**, 1066 (1990).
[37] R. Allenspach, M. Stampanoni, and A. Bischof, Phys. Rev. Lett. **65**, 3344 (1990).
[38] G. Bochi, C. A. Ballentine, H. E. Inglefield, S. S. Bogomolov, C. V. Thompson, and R. C. O'Handley, MRS Symposia Proceedings No. 313 (Materials Research Sociaty, Pittsburgh, 1993), p. 309.
[39] F. Huang, M. T. Kief, G. J. Mankey, and R. F. Willis, Phys. Rev. B **49**, 3962 (1994).
[40] G. Bochi, C. A. Ballentine, H. E. Inglefield, C. V. Thompson, R. C. O'Handley, H. J. Hug, B. Stiefel, A. Moser, and H. J. Guntherodt, Phys. Rev. B **52**, 7311 (1995).
[41] G. Bochi, H. J. Hug, D. I. Paul, B. Stiefel, A. Moser, I. Parashikov, H. J. Guntherodt, and R. C. O'Handley, Phys. Rev. Lett. **75**, 1839 (1995).
[42] G. Bochi, C. A. Ballentine, H. E. Inglefield, C. V. Thompson, and R. C. O'Handley, Phys. Rev. B **53**, R1729 (1996).
[43] M. T. Johnson P. J. C H. Bloemen, F. J. A den Broeder, and J. J. de Vries, Rep. Prog. Phys. **59**, 1409 (1996).
[44] D. Sander, Rep. Prog. Phys. **62**, 809 (1999).
[45] D. Sander, J. Phys.: Condens. Matter **16**, R603 (2004).
[46] B. N. Engel, C. D. England, R. A. Van Leeuwen, M. H. Wiedmann, and C. M. Falco, Phys. Rev. Lett. **67**, 1910 (1991).
[47] G. Bochi, O. Song, and R. C. O'Handley, Phys. Rev. B **50**, 2043 (1994).
[48] M. T. Johnson, R. Jungblut, P. J. Kelly, and F. J. A. den Broeder, J. Magn. Magn. Mater. **148**, 118 (1995).
[49] M. Hehn, S. Padovani, K. Ounadjela, and J. P. Bucher, Phys. Rev. B **54**, 3428 (1996).
[50] J. Prokop, D. A. Valdaitsev, A. Kukunin, M. Pratzer, G. Schonhense, and H. J. Elmers, Phys. Rev. B **70**, 184423 (2004).
[51] R. F. C. Farrow, D. Weller, R. F. Marks, M. F. Toney, S. Horn, G. R. Harp, and A. Cebollada, Appl. Phys. Lett. **69**, 1166 (1996).
[52] V. Gehanno, A. Marty, B. Gilles, and Y. Samson, Phys. Rev. B **55**, 12552 (1997).
[53] Y. Samson, A. Marty, R. Hoffmann, V. Gehanno, and B. Gilles, J. Appl. Phys. **85**, 4604 (1999).
[54] K. Oikawa, G. W. Qin, T. Ikeshoji, O. Kitakami, Y. Shimada, K. Ishida, and K. Fukamichi, J. Magn. Magn. Mater. **236**, 220 (2001).
[55] C. J. Sun, G. M. Chow, J. P. Wang, E. W. Soo, and J. H. Je, J. Appl. Phys. **93**, 8725 (2003).
[56] P. Glijer, J. M. Sivertsen, and J. H. Judy, J. Appl. Phys. **73**, 5563 (1993).
[57] W. K. Shen, A. Das, M. Racine, R. Cheng, J. H. Judy, and J. P. Wang, IEEE Trans. Magn. **42**, 2945 (2006).
[58] H. Tanigawa, K. Kondou, T. Koyama, K. Nakano, S. Kasai, N. Ohshima, S. Fukami, N. Ishiwata, and T. Ono, Appl. Phys. Express **1**, 011301 (2008).
[59] T. A. Moore, I. M. Miron, G. Gaudin, G. Serret, S. Auffret, B. Rodmacq, A. Schuhl, S. Pizzini, J. Vogel, and M. Bonfim, Appl. Phys. Lett. **93**, 262504 (2008).
[60] S. B. Choe, Appl. Phys. Lett. **92**, 062506 (2008).
[61] E. S. Lyons, R. C. O'Handley, and C. A. Ross, J. Appl. Phys. **95**, 6711 (2004).
[62] E. S. Lyons, R. C. O'Handley, and C. A. Ross, J. Appl. Phys. **99**, 08R105 (2006).
[63] S. G. Lee, S. W. Shin, J. W. Jang, H. M. Hwang, H. K. Jang, J. Lee, J. H. Lee, J. H. Song, J. Y. Choi, and H. S. Lee, J. Appl. Phys. **99**, 08Q513 (2006).
[64] M. Ciria, F. J. Castano, J. L. Diez-Ferrer, J. I. Arnaudas, B. G. Ng, R. C. O'Handley, and C. A. Ross, Phys. Rev. B **80**, 094417 (2009).
[65] A. Maziewski, V. Zablotskii, and M. Kisielewski, Phys. Rev. B **73**, 134415 (2006).
[66] S. H. Lee, F. Q. Zhu, C. L. Chien, and N. Markovic, Phys. Rev. B **77**, 132408 (2008).
[67] F. Ilievski, J. C. Perkinson, and C. A. Ross, J. Appl. Phys. **101**,

09D116 (2007).
[68] F. Ilievski, C. A. Ross, and G. J. Vancso, J. Appl. Phys. **103**, 07C520 (2008).
[69] N. Inaba, Y. Uesaka, and M. Futamoto, IEEE Trans. Magn. **36**, 54 (2000).
[70] H. Y. Sun, J. Hu, Z. F. Su, J. L. Xu, and S. Z. Feng, IEEE Trans. Magn. **42**, 1782 (2006).
[71] S. Chikazumi, *Physics of Ferromagnetism*, 2nd ed. (Oxford, New York, 1997).
[72] Free software at http://www.nanotec.es. A description of the software performance can be found in I. Horcas, R. Fernandez, J. M. Gomez-Rodriguez, J. Colchonero, J. Gomez-Herrero, and A. M. Baro, Rev. Sci. Instrum. **78**, 013705 (2007).
[73] B. Kaplan and G. A. Gehring, J. Magn. Magn. Mater. **128**, 111 (1993).
[74] V. Gehanno, Y. Samson, A. Marty, B. Gilles, and A. Chamberod, J. Magn. Magn. Mater. **172**, 26 (1997).
[75] C. Kooy and U. Enz, Philips Res. Rep. **15**, 7 (1960).
[76] T. Keitoku, J. Ariake, N. Honda, and K. Ouchi, J. Magn. Magn. Mater. **235**, 34 (2001).
[77] D. Clarke, O. A. Tretiakov, and O. Tchernyshyov, Phys. Rev. B **75**, 174433 (2007).
[78] S. P. Li, D. Peyrade, M. Natali, A. Lebib, Y. Chen, U. Ebels, L. D. Buda, and K. Ounadjela, Phys. Rev. Lett. **86**, 1102 (2001).
[79] J. Rothman, M. Klaui, L. Lopez-Diaz, C. A. F. Vaz, A. Bleloch, J. A. C. Bland, Z. Cui, and R. Speaks, Phys. Rev. Lett. **86**, 1098 (2001).
[80] M. Kläui, J. Rothman, L. Lopez-Diaz, C. A. F. Vaz, J. A. C. Bland, and Z. Cui, Appl. Phys. Lett. **78**, 3268 (2001).
[81] M. Kläui, C. A. F. Vaz, J. A. C. Bland, E. H. C. P. Sinnecker, A. P. Guimaraes, W. Wernsdorfer, G. Faini, E. Cambril, L. J. Heyderman, and C. David, Appl. Phys. Lett. **84**, 951 (2004).
[82] M. Steiner and J. Nitta, Appl. Phys. Lett. **84**, 939 (2004).
[83] F. J. Castaño, C. A. Ross, C. Frandsen, A. Eilez, D. Gil, H. I. Smith, M. Redjdal, and F. B. Humphrey, Phys. Rev. B **67**, 184425 (2003).
[84] F. J. Castaño, D. Morecroft, and C. A. Ross, Phys. Rev. B **74**, 224401 (2006).
[85] C. Nam, B. G. Ng, F. J. Castano, and C. A. Ross, J. Appl. Phys. **105**, 033918 (2009).
[86] C. L. Platt, K. W. Wierman, E. B. Svedberg, T. J. Klemmer, J. K. Howard, and D. J. Smith, J. Magn. Magn. Mater. **247**, 153 (2002).
[87] X. Liu, Z. Li, W. Shi, S. Li, F. Wei, D. Wei, and X. Liu, J. Appl. Phys. **105**, 07D503 (2009).
[88] C. Chappert and P. Bruno, J. Appl. Phys. **64**, 5736 (1988).
[89] H. Fritzsche, J. Kohlhepp, and U. Gradmann, Phys. Rev. B **51**, 15933 (1995).
[90] I. S. Lee, H. Ryu, H. J. Lee, and T. D. Lee, J. Appl. Phys. **85**, 6133 (1999).
[91] P. H. Townsend and T. A. Brunner, J. Appl. Phys. **62**, 4438 (1987).
[92] C. H. Hsueh, J. Appl. Phys. **91**, 9652 (2002).
[93] M. Y. Im, J. R. Jeong, and S. C. Shin, J. Appl. Phys. **97**, 10N110 (2005).
[94] K. Ha and R. C. O'Handley, J. Appl. Phys. **85**, 5282 (1999).
[95] M. Kisielewski, A. Maziewski, M. Tekielak, J. Ferre, S. Lemerle, V. Mathet, and C. Chappert, J. Magn. Magn. Mater. **260**, 231 (2003).
[96] L. Benito, J. I. Arnaudas, M. Ciria, C. de la Fuente, A. del Moral, R. C. C. Ward, and M. R. Wells, Phys. Rev. B **70**, 052403 (2004).
[97] R. C. O'Handley and S. W. Sun, J. Magn. Magn. Mater. **104-107**, 1717 (1992).
[98] R. Koch, M. Weber, K. Thurmer, and K. H. Rieder, J. Magn. Magn. Mater. **159**, L11 (1996).
[99] T. Gutjahr-Löser, D. Sander, and J. Kirschner, J. Magn. Magn. Mater. **220**, L1 (2000).
[100] A. Aharoni, J. Appl. Phys. **83**, 3432 (1998).
[101] R. Z. Lei, W. Tsai, I. Aberg, T. B. O'Reilly, J. L. Hoyt, D. A. Antoniadis, H. I. Smith, A. J. Paul, M. L. Green, J. Li, and R. Hull, Appl. Phys. Lett. **87**, 251926 (2005).
[102] A. N. Dobrynin, D. N. Ievlev, K. Temst, P. Lievens, J. Margueritat, J. Gonzalo, C. N. Afonso, S. Q. Zhou, A. Vantomme, E. Piscopiello, and G. Van Tendeloo, Appl. Phys. Lett. **87**, 012501 (2005).
[103] B. H. Miller and E. Dan Dahlberg, Appl. Phys. Lett. **69**, 3932 (1996).
[104] V. L. Mironov, B. A. Gribkov, S. N. Vdovichev, S. A. Gusev, A. A. Fraerman, O. L. Ermolaeva, A. B. Shubin, A. M. Alexeev, P. A. Zhdan, and C. Binns, J. Appl. Phys. **106**, 053911 (2009).